Toward Simultaneous Neurostimulation and Prosthetic Control: Real-Time Filtering of Amplitude-Modulated Stimulation Artifacts From Implanted Electrode Signals

Fabian Just, *Member, IEEE*, Roberta Reho, *Student Member, IEEE*, Max Ortiz-Catalan, and Eric J. Earley, *Member, IEEE*

***Abstract*— Restoring tactile feedback via nerve stimulation is essential for intuitive prosthetic control, yet the electrical artifacts introduced by stimulation pulses—especially with modulating amplitudes—can severely distort electromyographic (EMG) signals and impair decoding accuracy. This challenge is particularly critical in implanted neuromuscular interfaces, where the proximity of stimulating and recording electrodes can increase and magnitude of these signal artifacts. We present a real-time filtering algorithm that adaptively models and subtracts stimulation artifacts from implanted EMG electrode signals by using sample-wise polynomial regression based on stimulation amplitude. The algorithm was implemented on an embedded controller and evaluated in a participant implanted with a long-term neuromusculoskeletal interface compromising an osseointegrated implant for skeletal attachment, intramuscular and epimysial electrodes for prosthetic control enhanced with targeted muscle reinnervation (TMR), and a nerve cuff electrode for sensory feedback. The filter significantly restored key EMG feature distributions in offline tests across multiple movement classes. In real-time motion classification tasks, it improved movement completion rates from 20% to 60% under fixed stimulation and from 32% to 44% under amplitude-modulated stimulation. These findings demonstrate the algorithm's potential for recovering decoding performance during dynamic stimulation and validate its future use in advanced closed-loop prosthetic systems. This work addresses a longstanding barrier to integrating sensory feedback and motor control and provides a foundation for robust, real-world application of bidirectional prostheses using implanted interfaces.**

***Index Terms*— Prosthesis control, EMG signal processing, neuroprosthetics, nerve stimulation, osseointegration, neurostimulation, artifact removal.**

Received 15 June 2025; revised 19 November 2025 and 14 February 2026; accepted 25 March 2026. Date of publication 3 April 2026; date of current version 22 April 2026. Associate Editor: Erik Scheme. The work of Fabian Just, Max Ortiz-Catalan, and Eric J. Earley was supported in part by the Promobilia Foundation and in part by the IngaBritt and Arne Lundbergs Foundation. *(Fabian Just and Roberta Reho contributed equally to this work.) (Corresponding author: Fabian Just.)*

This work involved human subjects or animals in its research. Approval of all ethical and experimental procedures and protocols was granted by the Swedish Regional Ethical Committee, Gothenburg, Sweden, under Approval No.: DNR: 769-12.

Fabian Just is with the Electrical Engineering Department, Chalmers University of Technology, 412 96 Gothenburg, Sweden, and also with the Institute of Biomedical Engineering, Department of Engineering, Informatics and Psychology, Ulm University, 89081 Ulm, Germany (e-mail: just@chalmers.se).

Roberta Reho is with the Istituto di BioRobotica, Scuola Superiore Sant'Anna, 56025 Pisa, Italy (e-mail: Roberta.Reho@santannapisa.it).

Max Ortiz-Catalan is with the Prometei Pain Rehabilitation Center, 21018 Vinnytsia, Ukraine, and also with the Center for Complex Endoprosthetics, Osseointegration, and Bionics, 04136 Kyiv, Ukraine (e-mail: maxortizc@outlook.com).

Eric J. Earley is with the Department of Orthopedics and the Bone-Anchored Limb Research Group, University of Colorado Anschutz Medical Campus, Aurora, CO 80045 USA (e-mail: eric.earley@cuanschutz.edu).

Digital Object Identifier 10.1109/TNSRE.2026.3680643

I. Introduction

THE loss of an upper limb due to traumatic injury, cancer, or congenital deficiency significantly impacts an individual's functional capabilities and quality of life. The field of upper limb prosthetics has evolved considerably, transitioning from body-powered mechanisms—operated via mechanical cables and harnesses—to surface myoelectric prostheses that leverage electromyographic (EMG) signals for more intuitive control [1], [2], [3].

However, major challenges remain, particularly the absence of natural tactile and proprioceptive feedback [4], difficulty in acquiring stable EMG signals [5], and discomfort associated with traditional socket-based prosthetic attachments [6]. Many people with amputations experience skin irritation, pressure-related pain, and limitations in movement due to the constraints of socket prostheses, often leading to device abandonment in favor of simpler alternatives [7]. Moreover, EMG-based prosthetic control faces significant challenges due to signal quality being affected by environmental factors like temperature and humidity, skin-related factors, motion artifacts, and myoelectric crosstalk [8]. Osseointegration offers a transformative solution to these issues by providing a direct skeletal attachment for prosthetic limbs. Unlike conventional socket-based prosthetics, an osseointegrated implant

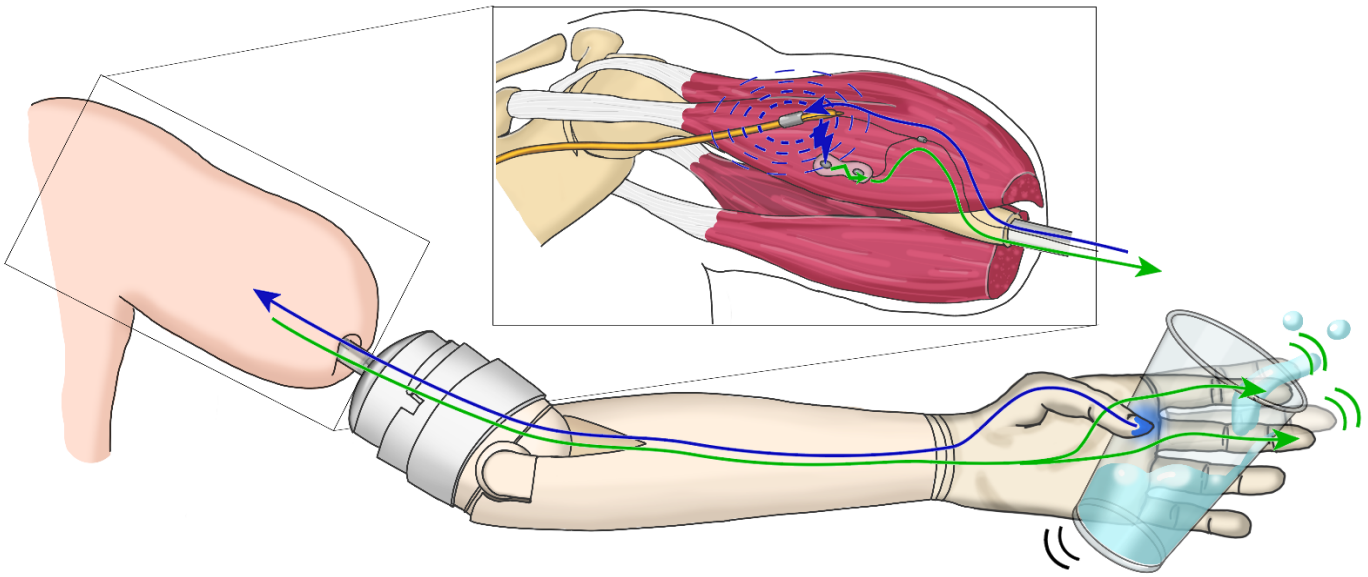

Fig. 1. Simultaneous nerve stimulation and EMG decoding in an osseointegrated prosthetic user. Electrical stimulation (blue) delivered through a nerve cuff induces artifacts in implanted EMG recordings (green), leading to signal distortion, classification errors, and unintended prosthetic movements.

eliminates the need for a socket, significantly enhancing comfort, stability, and mobility. This integration not only improves mechanical stability but also enables the use of implanted electrodes—such as intramuscular, epimysial, and extra-neural spiral-cuff electrodes—offering greater signal reliability and control precision compared to surface EMG electrodes, which are susceptible to movement artifacts, sweat, temperature variations, and skin impedance fluctuations [8], [9]. Studies have demonstrated that prosthetic function, usability, and long-term acceptance have markedly improved in osseointegrated prosthesis users, especially when combined with advanced surgical techniques such as targeted muscle reinnervation (TMR) [10], [11], [12].

TMR reroutes residual nerves from the amputated limb to alternative muscle sites, allowing users to control their prosthesis through natural muscle contractions. This technique facilitates a more intuitive and responsive control interface, particularly when paired with implanted electrodes, which offer at least ten times greater signal reliability compared to surface sensors [13], [14], [15], [16]. The combination of osseointegration, TMR, and implanted electrodes forms an advanced interface between the user's nervous system and the prosthetic limb, supporting bidirectional communication through both motor intent decoding and artificial sensory feedback [8], [9].

By modulating stimulation for sensory feedback—particularly stimulation amplitude [17]—it is possible to convey graded sensations of pressure and contact intensity. However, this introduces a critical technical challenge: stimulation pulses typically have higher amplitudes than natural EMG signals and produce artifacts that contaminate the recorded signals from implanted electrodes (Fig. 1). These artifacts distort the recorded EMG and thus, interfere with movement classification algorithms ultimately compromising prosthetic control [18], [19]. The simultaneous use of nerve stimulation and prosthetic control is essential for closed-loop systems, yet remains challenging in real-world applications. Previous attempts to address stimulation artifacts focused on static or fixed-pattern stimulation scenarios [19]. However, these approaches fail under more naturalistic conditions, where tactile interactions are dynamic and stimulation amplitudes must continuously adapt. As such, the need for artifact rejection methods that remain robust under amplitude-modulated stimulation is clear.

Although artifact rejection has been explored in other areas of neurotechnology—such as EEG [20], local field potentials [21], Bidirectional Brain-Computer Interfaces (BCIs) [22], closed-loop neuromodulation [23], and ECG-EMG interference [24], [25] —these methods are not optimized for the demands of prosthetic control using implanted EMG.

To address this gap, this study proposes a novel real-time filtering algorithm designed to remove amplitude-modulated stimulation artifacts from EMG control signals in an embedded prosthesis controller. The algorithm dynamically adapts to changes in stimulation amplitude and waveform morphology, enabling template subtraction of the modeled artifacts without distorting underlying myoelectric signals. Its effectiveness is evaluated both offline and in real-time using data from a prosthesis user with an osseointegrated implant and implanted electrodes.

The results demonstrate that the proposed approach recovers critical EMG information, significantly improves classification accuracy, and can facilitate simultaneous control and sensory feedback. This work contributes to the development of next-generation closed-loop neuroprostheses and supports enhanced function and quality of life for individuals with advanced prosthetic systems.

II. Materials and Methods

This work includes two studies performed with a participant implanted with an osseointegrated neuromusculoskeletal prosthesis. The first study involved offline signal analysis;

the second assessed real-time performance during functional control tasks.

A. Participant and Implant Configuration

This study was conducted with a participant who had undergone a transhumeral amputation following traumatic injury. The individual was implanted with a neuromusculoskeletal interface (e-OPRA, Integrum AB, Sweden) which provides a direct skeletal attachment for the prosthesis and a bidirectional electronic interface with implanted neuromuscular electrodes [12]. All procedures were approved by the Regional Ethical Review Board in Gothenburg (Dnr. 18-T125), and written informed consent was obtained prior the investigations.

Surgical reconstruction included the implantation of a titanium fixture in the humerus, followed by the creation of electro-neuromuscular constructs. The three major nerves of the brachial plexus—median, ulnar, and radial—were surgically dissected into fascicles. These fascicles were transferred to reinnervate both native denervated muscles and non-vascularized free muscle grafts harvested from the thigh. Intramuscular and epimysial electrodes were implanted in reinnervated and unreconstructed muscles, and a multi-contact nerve cuff electrode was placed around one fascicle of the median nerve for sensory stimulation. The internal wiring was routed through the osseointegrated implant using feedthrough technology, enabling chronic access to EMG signals and stimulation pathways.

At the time of the present experiments, the full neuromusculoskeletal system had been in continuous use for over four years, providing a stable and mature interface for both control and feedback [12].

B. System Overview: Hardware and Signal Pathway

The system used to implement the artifact filter and to coordinate communication between the implanted interface and the prosthetic hand is a dedicated embedded controller developed for neuromusculoskeletal prosthetic applications. It acts as the bridge between the e-OPRA implant system and a myoelectric prosthetic hand, handling both signal acquisition and stimulation control. The controller manages these functions in real-time, enabling synchronized delivery of nerve stimulation and recording of EMG signals from implanted electrodes. This setup supports the simultaneous use of motor control and sensory feedback, which is essential for closed-loop prosthetic operation.

During electrical stimulation, the secondary microcontroller temporarily disables EMG signal recording — a process known as *blanking*. The number of EMG samples blanked depends on the pulse width of the stimulation. While this approach effectively removes the sharp peak of the stimulation artifact (the "acute phase"), it does not eliminate the longer signal tail that remains after the pulse. The duration and size of this residual artifact tail vary depending on both the stimulation amplitude and the pulse width [18], [23], [26].

C. Stimulation Artifact Challenge and Filter Overview

Simultaneous myoelectric control and sensory feedback is a key enabler of natural, intuitive prosthesis use. However, neurostimulation artifacts are particularly problematic in neuromusculoskeletal prostheses, where electrodes implanted in muscles for control purposes are in close proximity to the stimulation site by neural electrodes.

In these systems, stimulation artifacts often exceed the amplitude of natural EMG signals by an order of magnitude, leading to contamination of motor intent information and misclassification of intended movements. The challenge is exacerbated when stimulation parameters—especially amplitude—are modulated in real time to provide graded sensory feedback. Under such conditions, the amplitude of the artifact vary continuously, complicating artifact removal.

Static or adaptive artifact subtraction methods may be able to mitigate stimulation artifacts that are not proportionally modulated for example, discrete event-driven sensory feedback [27]. However, if stimulation parameters modulate e.g. with grasping force, then their performance will deteriorate, as the artifact template will either not modulate with stimulation or will continuously lag behind the current stimulation setting. To address this limitation, we developed a novel filtering approach based on adaptive artifact modeling. The method generates a customized template for each stimulation pulse in real time, using information about the current stimulation amplitude and fixed pulse width. This template is then subtracted from the recorded EMG signal, enabling simultaneous control and feedback. The following section details the algorithmic implementation of this approach.

D. Adaptive Artifact Subtraction

The filtering algorithm is based on two key assumptions:

1. The general temporal pattern of the artifact remains consistent regardless of stimulation amplitude or pulse width, supporting the assumption that the same artifact subtraction approach can be extended to modulating pulse width at a fixed amplitude, as well as modulating amplitude.
2. The amplitude of the artifact scales proportionally with the modulated stimulation parameter (e.g. amplitude or pulse width) while the other parameter is kept fixed [28]

These assumptions allow for the generation of a real-time artifact template that is specific to each stimulation pulse. During a calibration phase, stimulation was applied while the participant's limb was at rest to isolate artifact waveforms. The stimulation parameters were fixed in frequency and pulse width, while amplitude was varied across five levels (300–500 μA) to sample the dynamic range of artifact shapes. These recordings provided clean artifact examples without the influence of voluntary EMG activity.

Each artifact was segmented and time-aligned to stimulation onset, creating a set of template waveforms for each stimulation amplitude. Each template was grouped and labeled according to the corresponding stimulation current (Fig. 2). For each sample index i, the recorded signal values across amplitudes were used to train a regression model of the artifact ($\hat{\varepsilon}$). Although linear regression was initially considered, the relationship between stimulation amplitude and artifact magnitude exhibited non-linear trends. As a result, a third-order

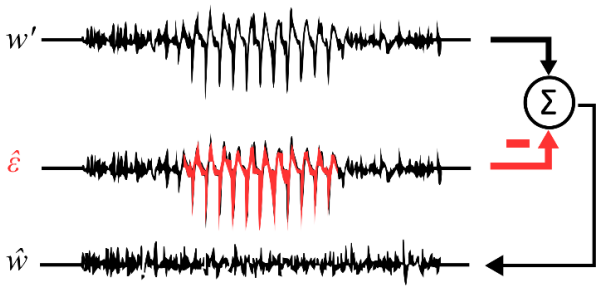

Fig. 2. Stimulation artifact rejection (SAR) using adaptive template subtraction. The EMG signal (top) is distorted by stimulation artifacts resulting from amplitude-modulated pulses. For each pulse delivered by the ALC, the corresponding stimulation current is known. Using this information, the filtering algorithm computes the appropriate artifact value at each sample point by evaluating the regression models and subtracts it from the incoming EMG signal in real time, yielding a cleaned signal suitable for classification.

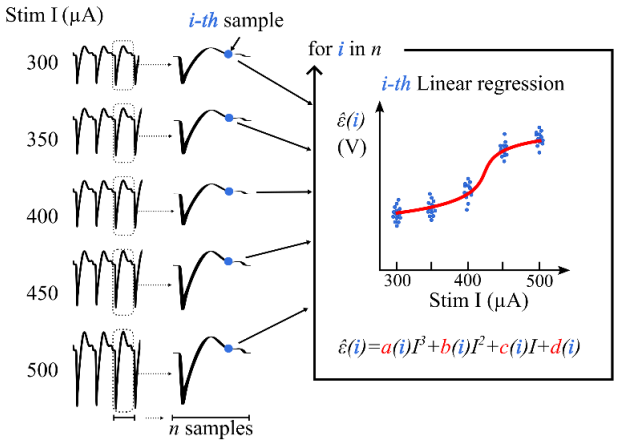

Fig. 3. Artifact modeling using polynomial regression. Neurostimulation pulses at various current amplitudes (300-500 μA) are delivered through the active cuff, and the resulting stimulation artifacts are recorded via EMG channels. Templates of the pulse artifacts are segmented, classified by amplitude, and used to fit a third-order polynomial regression for each sample in the artifact window. The result is a set of n regression models—one per sample—each describing how the artifact amplitude varies with stimulation intensity. These models are stored and later used to generate adaptive templates for real-time artifact subtraction.

polynomial regression was employed to estimate each sample:

$$\hat{\varepsilon}(i) = a(i)A^3 + b(i)A^2 + c(i)A + d(i) \quad (1)$$

Here, A represents the stimulation amplitude (in μA), and $a(i)$, $b(i)$, $c(i)$, and $d(i)$ are the liner regression coefficients corresponding to the i-th sample of the estimated artifact waveform. The result is a set of per-sample models capable of generating a complete artifact template for any stimulation amplitude within the calibrated range.

During real-time operation, the system activates upon the onset of each stimulation pulse and retrieves the current amplitude from the control stream. Using Equation (1), the algorithm reconstructs the expected artifact waveform sample-by-sample. This template ($\hat{\varepsilon}$) is then subtracted from the measured EMG signal (w'):

$$\hat{w}(i) = w'(i) - \hat{\varepsilon}(i) \quad (2)$$

where $w'(i)$ is the i-th sample of the recorded EMG signal and $\hat{w}(i)$ is the i-th sample of the estimated cleaned output. This process allows for removal of both the peak and tail components of the artifact while preserving the underlying myoelectric information.

The subtraction is executed immediately after the stimulation pulse ends (Fig. 3). The algorithm then iterates through each sample index, computes the predicted artifact value from the stored polynomial coefficients, and subtracts it from the corresponding EMG sample.

This real-time implementation is computationally-efficient and supports artifact subtraction at a resolution of 10 μA across the range of 300–500 μA, enabling robust operation during amplitude-modulated sensory feedback. The integration of this algorithm into an embedded controller enables closed-loop prosthetic systems to function effectively under conditions where artifact contamination would otherwise compromise control accuracy.

E. Implementation: Training & Deployment

To accommodate user-specific stimulation profiles, the stimulation artifact rejection (SAR) filtering algorithm is trained individually for each user under controlled conditions. The system assumes a fixed stimulation pulse width while allowing amplitude modulation. Therefore, regression models must be calibrated offline prior to deployment. A MATLAB-based tool was developed to streamline this process, which includes data preprocessing, model fitting, and parameter export for both offline and embedded use.

The training and deployment pipeline consists of the following phases and is illustrated in Figure 4:

1) Artifact Segmentation and Preprocessing: Artifact recordings are acquired at multiple stimulation amplitudes while the limb remains at rest. These signals are segmented into individual artifact templates aligned with the onset of each stimulation pulse. Blanked samples—introduced by the controller to suppress acute stimulation peaks—are used to identify pulse timing. Outlier pulses are detected and removed to ensure robust model fitting. The remaining templates are organized into matrices, one for each stimulation amplitude.
2) Regression Model Fitting: For each sample index in the artifact window, signal values across all amplitude conditions are used to fit a third-order polynomial regression model. This process is repeated for all samples, resulting in a unique set of regression coefficients for each. These models capture how the artifact's amplitude evolves with changes in stimulation intensity, enabling accurate reconstruction during real-time filtering.
3) Parameter Export and Integration: The regression parameters—four coefficients per sample—are stored in channel-specific tables. These can be used in two contexts: (i) for offline filtering in MATLAB, where the algorithm reconstructs the artifact waveform based on pulse amplitude and subtracts it from the EMG signal, and (ii) for real-time operation on the ALC.

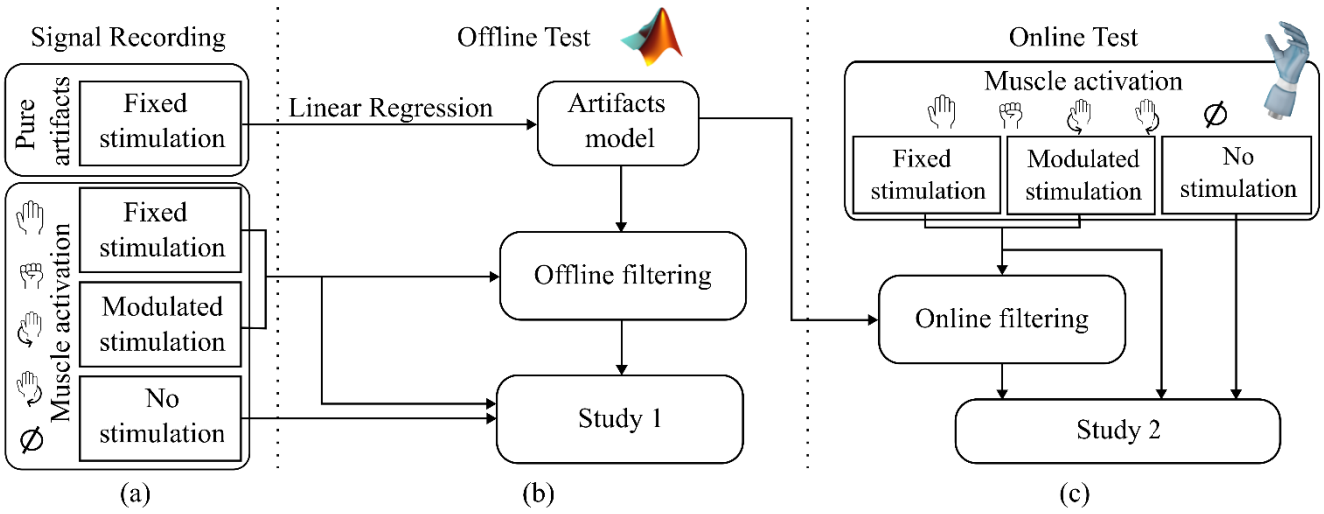

Fig. 4. Overview of study phases. a) Signal acquisition: artifact recordings (stimulation without EMG) and voluntary EMG recordings with and without stimulation. b) Offline testing: artifact templates were used to build a regression-based model, applied to filter EMG signals; features from unperturbed, corrupted, and filtered signals were extracted and compared. c) Real-time testing (motion test): motion classification tasks were performed to evaluate filter performance under dynamic stimulation conditions online.

As shown in Figure 3, the embedded controller retrieves the stimulation amplitude for each pulse, computes the artifact template using the pre-trained regression models, and subtracts it from the recorded EMG signal in real time. This enables adaptive artifact suppression at the resolution of 10 μA across the 300–500 μA range.

The generated parameters can be utilized in MATLAB for offline filtering. The algorithm detects the pulse cue, predicts the artifact sample for each pulse based on its amplitude using the corresponding model, and subtracts it from the original EMG signal to recover the clean signal.

Additionally, these parameters can be loaded onto the ALC firmware via Bluetooth and stored in RAM. During real-time filtering, the firmware retrieves the relevant coefficients and reconstructs the artifact waveform sample by sample. Each parameter is stored as a 32-bit floating-point value, and the third-order regression model requires four coefficients per sample. With a sampling rate of 500 Hz and a stimulation frequency of 20 Hz, typical artifact templates contain 21–23 samples. As a result, the average memory requirement for storing the coefficients across all channels is approximately 1.4 kB, making this solution both precise and memory-efficient for embedded implementation.

F. Study 1–Offline Signal Recovery and Artifact Suppression

To investigate the effects of neurostimulation artifacts on EMG signal quality—and to evaluate the capability of the proposed SAR filter to restore signal integrity—we conducted a dedicated offline experimental study with a participant implanted with an osseointegrated neuromusculoskeletal prosthesis. This study involved a series of controlled stimulation and movement conditions designed to simulate realistic prosthesis use while allowing artifact quantification and feature-level analysis.

Recordings were acquired from four intramuscular and epimysial EMG channels under structured experimental conditions involving both stimulation and voluntary muscle activation. The participant was instructed to perform four motor tasks: open hand, close hand, pronation, and supination—under three stimulation conditions:

1) Baseline (no stimulation)
2) Fixed stimulation (constant amplitude)
3) Amplitude-modulated stimulation (variable amplitude)

In addition, stimulation-only trials were performed while the limb remained at rest to isolate pure stimulation artifacts, which later served as reference signals for filter calibration. All data were collected in a seated, stable position. The complete structure of the study protocol is outlined in Figure 4a, which shows the recording stages for both EMG and artifact signals.

Each recording lasted six seconds to stay within established safety limits for continuous electrical stimulation. Fixed stimulation consisted of 100 pulses delivered at 20 Hz, with a pulse width of 300 μs and a constant amplitude of 300 μA. For modulated stimulation trials, a pre-defined sequence of pressure values was delivered as sensory feedback.

These values were derived from force sensor readings recorded during functional grasping tasks and mapped to stimulation amplitudes in the 300–500 μA range. Although the amplitude varied dynamically in this condition, the pulse width (300 μs) and frequency (20 Hz) remained fixed.

Figure 5 presents representative traces of both fixed and modulated stimulation patterns, highlighting how amplitude modulation introduces variability in artifact magnitude and waveform shape—critical for evaluating filter performance under dynamic sensory feedback scenarios.

Following data collection, all EMG signals (both raw and filtered) were segmented into overlapping windows of 200 milliseconds, with a 150-millisecond overlap. From each window, the Hudgins four time-domain features were extracted [29]: Mean Absolute Value (MAV), Zero Crossings (ZC), Waveform

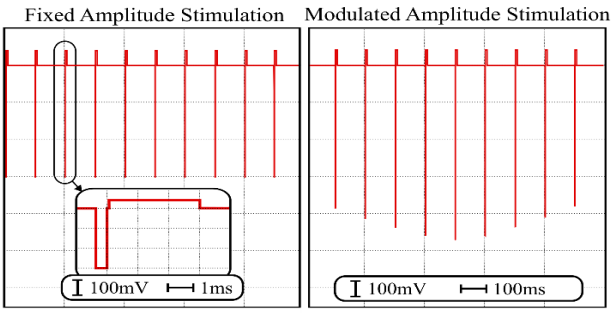

Fig. 5. Fixed and modulated stimulation pulses delivered at 20 Hz with 300 μs width. Fixed stimulation (left) used a constant 300 μA current, while modulated stimulation (right) varied between 300 and 500 μA, producing artifacts proportional in amplitude (300–500 mV).

Length (WL), Slope Sign Changes (SSC). These features were selected due to their widespread and standardized use in prosthetic pattern recognition. Among the Hudgins features, MAV provides the strongest classification power, owing to its high signal-to-noise ratio, direct proportionality to muscle activation, and robustness to contraction variability [30]. Comparing these features across the baseline, artifact-corrupted, and filtered recordings allowed us to quantify the extent of signal degradation caused by stimulation artifacts and assess the effectiveness of the proposed linear regression–based filtering approach in restoring functional signal characteristics. Additionally, the same recorded signals were filtered offline using the adaptive Template Subtraction (TS) algorithm presented in a previous study [19]. The TS algorithm builds an artifact template by recursively averaging the EMG samples that follow each stimulation pulse using multiple exponential (first-order IIR) updates. The learned template is then subtracted from the raw signal to obtain an estimate of the artifact-free EMG.

G. Study 2–Real-Time Decoding of Motor Intention With Sensory Feedback

To assess the functional impact of stimulation artifacts and the effectiveness of the proposed filter under real-time conditions, we conducted a standardized motion classification study with the same participant. The objective was to evaluate whether the artifact filter could restore reliable EMG decoding during simultaneous sensory stimulation, which subsequently can be used for closed-loop prosthetic control. The participant performed a set of five distinct motor tasks: rest, open hand, close hand, pronation, and supination. These movements were selected for their relevance in daily prosthesis use and were classified in real time using a myoelectric pattern recognition algorithm. Each test condition included five repetitions per movement class, executed in randomized order, for a total of 25 trials. A repetition was considered successful if the algorithm correctly classified the intended movement for a cumulative duration of one second within a five-second window.

The study followed the standardized online Motion Test protocol described by Kuiken et al. [31] adapted for e-OPRA users [32], who provide a validated method for quantifying

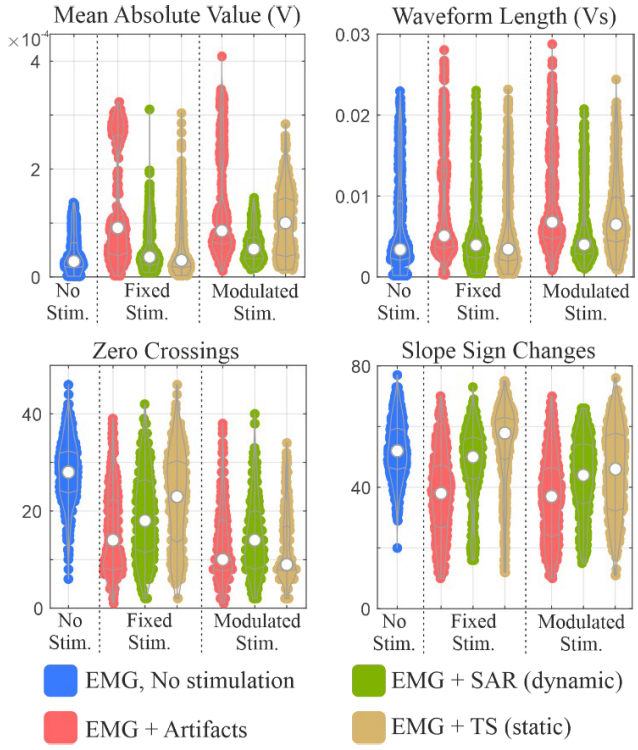

Fig. 6. Violin plots of all features aggregated across movement classes. Distributions for each feature (MAV, ZC, WL, SSC) are shown under five conditions: baseline (No Stim., blue), fixed stimulation (Fix Stim., red), and modulated stimulation (Mod Stim., red). The artifact removal filters are visualized with distinct colors: The SAR artifact removal filter (Fix S. +SAR and Mod S. +SAR) in green and the TS artifact removal filter (Fix S. + TS and Mod S. + TS) in gold.

prosthetic motion control performance under real-time constraints. The experiment included the following test conditions:

a) Baseline: No stimulation applied, serving as a reference for evaluating motor decoding.
b) Fixed stimulation: Electrical stimulation delivered at 20 Hz with a constant amplitude of 300 μA and a pulse width of 300 μs.
c) Modulated stimulation: Amplitudes varied dynamically between 300 and 500 μA, simulating graded sensory feedback while maintaining the same pulse width and frequency.
d) Fixed stimulation + filter: Same parameters as condition 2, with the artifact filter enabled.
e) Modulated stimulation + filter: Same parameters as condition 3, with the artifact filter enabled.

Each condition was tested independently, and within each test, the participant was instructed to perform the full set of movement tasks in randomized order. The classification algorithm's ability to detect and hold the correct movement class was logged alongside metrics such as completion time, selection time, and overall accuracy. The full protocol structure, including offline and real-time phases, is summarized in Figure 5. This study enabled a direct evaluation of the filter's real-time performance in restoring reliable decoding of motor intention in the presence of stimulation-induced artifacts—particularly under amplitude-modulated feedback scenarios that most closely reflect real-world use.

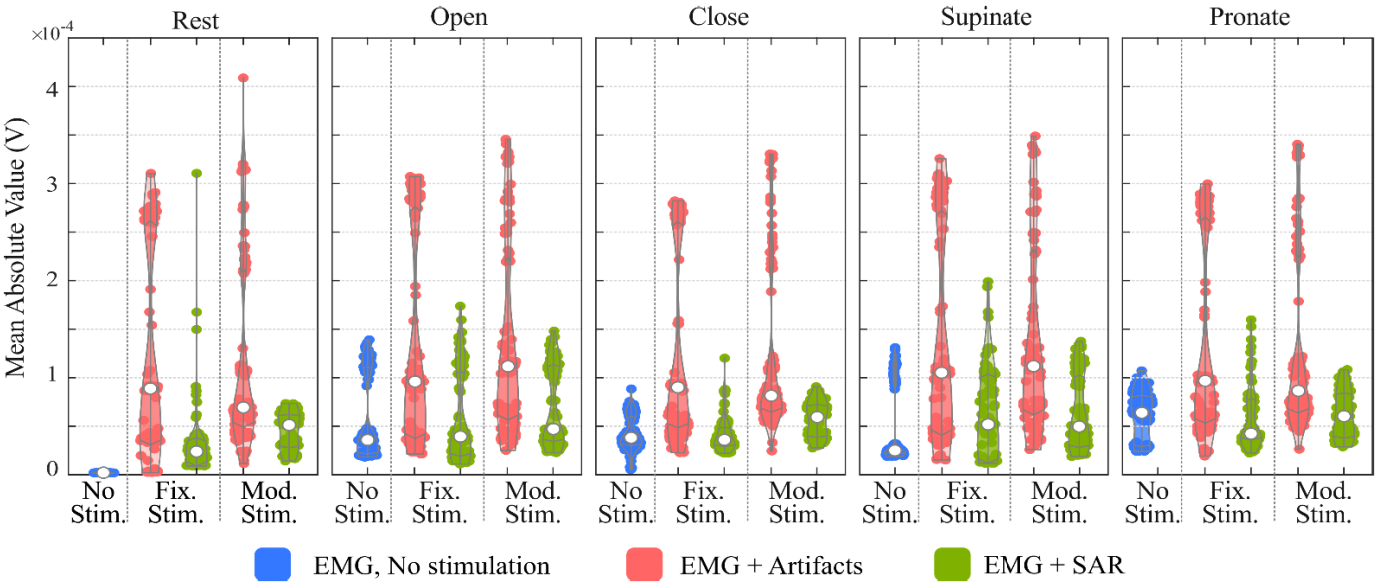

Fig. 7. Mean Absolute Value (MAV) feature distribution across movement classes. Distributions are shown for each movement (rest, open, close, pronation, and supination) under five signal conditions: no stimulation (No S.), fixed stimulation (Fix S.), modulated stimulation (Mod S.), and the corresponding filtered signals using the artifact removal method (Fix S. +SAR and Mod S. +SAR). The filter was implemented using a linear regression model.

III. Results

A. Study 1: Offline Evaluation of Artifact Suppression and Signal Recovery

The four time-domain EMG features were evaluated under five conditions: No Stimulation, Fixed Stimulation, Modulated Stimulation, and their filtered counterparts. Distributions were analyzed to assess the impact of stimulation and the effect of the artifact filter. Stimulation altered the distribution of all four features (Fig. 6). MAV increased under both fixed and modulated stimulation and was consistently reduced after filtering. ZC distributions shifted notably with stimulation, and filtering partially restored these values, especially in the fixed stimulation condition. WL also increased due to stimulation and decreased after filtering. SSC showed a reduction under stimulation, with partial recovery following filtering. Across all features, deviations from baseline were more pronounced under modulated stimulation than fixed. Filtering reduced these deviations in all cases, with stronger recovery seen in fixed stimulation conditions. Regarding MAV across individual movement classes, in the absence of stimulation, rest signals showed values close to zero, while active movements such as open, close, pronation, and supination produced MAV values in the order of 10^{-4}. Both fixed and modulated stimulation led to elevated MAV values compared to the no-stimulation condition across all classes. After filtering, the distributions for close, open, and pronation movements shifted notably back toward baseline levels. The violin plots of the filtered signals closely resembled those of the no-stimulation condition, with the large artifact-driven expansions—up to four times the size of the baseline distribution—reduced to a comparable range. Supination showed a partial reduction in MAV, while rest signals remained elevated, indicating that some residual artifact persisted during non-active periods (Fig. 7). Compared to the adaptive Template Subtraction solution [19], the SAR algorithm performed more efficiently in restoring the original distribution of the features, especially in the MAV and WL features and in the case of modulated stimulation.

B. Study: Real-Time Decoding of Motor Intention With Sensory Feedback

To assess the performance of the artifact filter in real-time conditions, motion classification tests were conducted under five stimulation modes: no stimulation, fixed stimulation, modulated stimulation, and the corresponding filtered conditions. Figure 8 shows movement-wise completion rates under each stimulation condition. Stimulation affected recognition performance unevenly across movement classes. Without stimulation, the participant achieved a 96% completion rate across movement classes. Completion rates dropped for all movements except open hand, which remained detectable in all conditions. While open hand classification was preserved even under artifact-heavy conditions, this outcome may reflect a classification bias induced by artifact patterns, rather than true EMG activation. In contrast, recognition of close hand, rest, and supination was suppressed by stimulation but recovered when the filter was applied. In the fixed stimulation condition, overall movement classification improved from 20% to 60% with the filter, representing a tripling in successful classifications. In the modulated condition, the filter enabled classification of one additional movement, increasing overall completion from 32% to 44%.

Performance was also evaluated using four metrics: completion rate, classification accuracy, completion time, and selection time. Classification accuracy (as shown in Figure 9), which had a median of 90% under baseline conditions, declined substantially under both stimulation types. With filtering enabled, partial recovery was observed, but accuracy did not return to baseline levels.

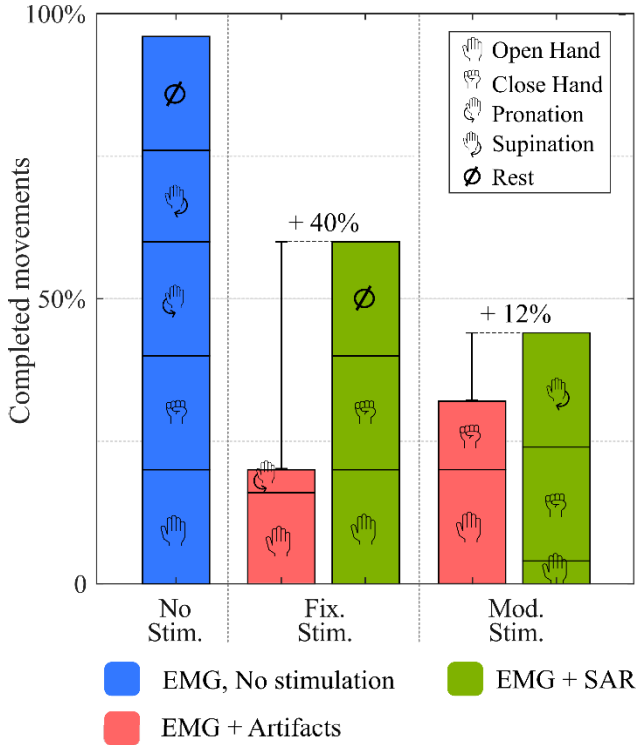

Fig. 8. Completion rates by movement class across stimulation conditions. Stacked bar plots showing the classification success rate for each movement under different stimulation modalities. With the filter enabled, fixed stimulation trials improved from 20% to 60% completion—effectively tripling the number of successful movement classifications. Under modulated stimulation, the filter enabled recognition of one additional movement class, increasing the overall completion rate by 12%.

Completion time, defined as the time required to correctly classify a movement for one second within a five-second trial window, increased markedly under stimulation. Without stimulation, classification occurred with the shortest possible delay (one second). In the stimulation conditions, most movements were not recognized within the timeout, except for the open hand. With the filter applied, completion time was fully restored for close hand movements under both stimulation types and for supination under modulated stimulation.

Selection time, which measures the latency from trial onset to the first correct classification, remained low in the no-stimulation condition. Under fixed stimulation without filtering, movements other than open hand were not identified. In the modulated condition, selection time was comparable to baseline, as the algorithm often detected correct movements before artifact levels rose. Filtering reduced selection time in fixed stimulation trials but had little additional effect in the modulated condition due to early classification during low-amplitude stimulation.

IV. Discussion

This study addressed a key challenge in closed-loop prosthetic systems: removing stimulation artifacts from EMG signals under conditions of amplitude-modulated nerve stimulation. Unlike previous studies that focused on static stimulation or surface EMG, we proposed and validated a method tailored to dynamic sensory feedback in implanted systems. Our regression-based algorithm models artifact waveforms at the sample level, enabling real-time subtraction of stimulation-dependent noise with high temporal resolution.

A. Suppression of Amplitude-Modulated Artifacts

Stimulation artifact suppression under amplitude modulation is a novel focus in this domain. Most existing techniques, including blanking and fixed template subtraction, are limited to uniform stimulation and do not accommodate real-time changes in amplitude. Our findings demonstrate that stimulation strongly disrupts signal characteristics, particularly under modulation, with feature distributions (e.g., MAV) expanding up to fourfold relative to baseline values (Fig. 7). These distortions significantly impair classification performance and make reliable prosthetic control unattainable for the user.

The proposed filter was able to reduce the artifact-driven widening of MAV distributions, shifting the measured features back in the direction of the baseline scale in three of the four tested movement classes. Specifically, for close, open, and pronation, the post-filtered distributions closely matched those from the no-stimulation condition, while rest signals retained elevated noise, likely due to low intrinsic EMG amplitude and sensitivity to residual high-frequency components.

Violin plots across all features (Fig. 6) further confirm these trends. Filtering produced substantial recovery of Mean Absolute Value, Waveform Length, and Slope Sign Changes. Zero Crossings showed the least improvement, particularly under modulated stimulation and in rest periods, suggesting limitations in capturing rapid signal polarity shifts in regions still affected by subtle residual noise. The limited recovery of zero-crossing features likely reflects residual high-frequency noise and is not unexpected given the sensitivity of ZC to minor waveform perturbations. The residual inconsistencies observed during rest likely reflect the inherently low signal-to-noise ratio in this condition, where small remaining artifacts disproportionately influence feature estimates. During active contractions, the clinically relevant scenario for prosthetic control, the filter consistently restored EMG feature quality and decoding performance. In the case of modulated stimulation, the proposed algorithm outperforms the previously proposed TS filter solution [19]. This improvement is expected, as the adaptive nature of TS makes it specifically suited to learn and reject a fixed waveform, whereas the present approach was explicitly developed to accommodate modulating waveforms.

B. Restoration of Real-Time Decoding of Motor Intent

The impact of artifact filtering on real-time control was reflected in improved classification performance across all measured metrics. Completion rates, which fell to 20% (fixed) and 32% (modulated) under unfiltered stimulation, increased to 60% and 44% respectively when filtering was applied (Fig. 8). This restoration enabled recovery of several movements that were otherwise completely inaccessible to the user during unfiltered stimulation, with a tripling of recognized movements under fixed stimulation, and recovery of one additional class under modulation. While this demonstrates clear benefit, we

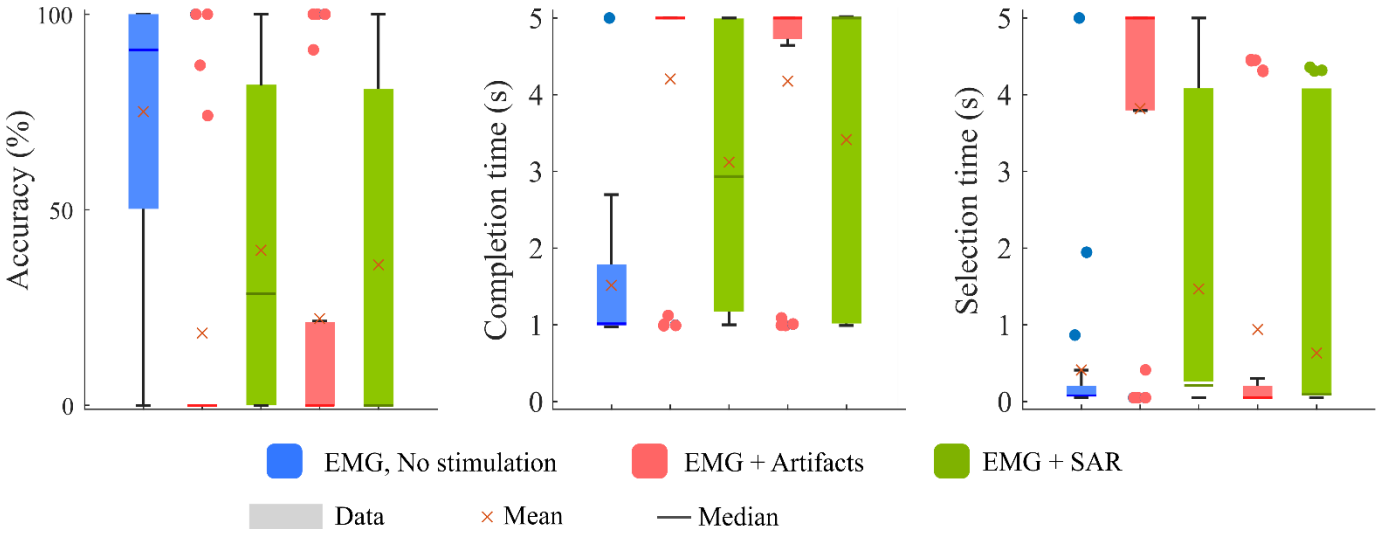

Fig. 9. Classification accuracy, completion time, and selection time across stimulation conditions. Performance metrics from motion tests conducted without stimulation (No S.), with fixed stimulation (Fix S.) and modulated stimulation (Mod S.), and with the application of the artifact removal filter (Fix S. +SAR and Mod S. +SAR). The filter, implemented using a linear regression model, substantially improved classification accuracy and reduced timing delays introduced by stimulation artifacts.

acknowledge that this method alone may not fully recover baseline performance. We therefore emphasize that artifact prevention (e.g., bipolar electrode configurations, optimized cuff placement) remains the ideal solution, with SAR serving as an important complementary tool when residual artifacts persist.

The proposed filter substantially improved classification performance and restored previously inaccessible movements, enabling meaningful functional gains in real-time prosthetic control. However, overall performance remained below baseline without stimulation, which may affect usability and require additional user adaptation. Further work is required to achieve maximal signal restoration and to characterize how this approach affects user behavior in daily life.

Without filtering, most movements could not be recognized within the timeout period, despite any control adaptations made by the user. Completion time was fully restored for close hand movements in both stimulation conditions and for supination in the modulated case. Selection time was reduced in fixed stimulation when filtering was active, although it remained unchanged in modulated trials, likely due to early correct classification during low-amplitude phases of stimulation.

Interestingly, the open hand movement was consistently detected in all conditions, including unfiltered stimulation. However, this likely reflects misclassification caused by the artifact waveform resembling the expected activation pattern, rather than successful decoding of motor intent, a critical observation highlighting the danger of uncorrected artifacts in pattern recognition systems.

C. Practical Considerations and Scalability

The filtering algorithm uses a third-order polynomial regression model for each sample in the artifact window, enabling continuous interpolation across a stimulation amplitude range of 300–500 μA with 10 μA resolution. By fitting the regression model separately to each sample, our algorithm is agnostic to the true temporal profile of the stimulation artifact, meaning that it can be easily applied to different electrodes without modification, even if the electrodes have different electrical impedances or proximity to neurostimulation sources.

Despite the per-sample complexity, the implementation remains lightweight, requiring only ~1.4 kB of RAM across four EMG channels.

This memory footprint was acceptable in the current embedded system, but it may become limiting when increasing the number of EMG channels, sampling rate, or introducing additional model complexity (e.g., multi-parameter regression for simultaneous amplitude and width modulation). To meet tighter memory constraints, further approximations could be explored—such as reducing the number of parameters, using piecewise lower-order fits, or employing coefficient quantization techniques. However, such approaches risk compromising precision, as has been observed in prior work on neurostimulation artifact modelling [33], [34]. Residual variability in artifact morphology, especially in rest conditions and for ZC features, indicates that external factors such as tissue impedance, electrode positions, and muscle tone influence the filter's effectiveness. In this study, limb position and contraction level were kept stable during calibration, but more variable real-world scenarios may require adaptive or user-specific adjustments to the filter.

D. Limitations and Future Work

This study was conducted with a single participant implanted with a neuromusculoskeletal prosthesis. Only six individuals in Sweden had the neuromusculoskeletal prosthesis used in this study, most of whom had no issues with stimulation artifacts. Thus, we took a patient-centered approach to addressing the challenges faced by the participant in this study, one which we believe can be applied to any individual facing similar challenges with simultaneous neurostimulation and prosthetic control. Although our results demonstrate the

feasibility of our approach for our participant, future work including participants with different amputation levels and electrode configurations are needed to confirm generalizability across anatomical and signal variations.

Limb position is known to affect myoelectric control in surface EMG systems [35], however its effect on stimulation artifacts is unclear. Implantable electrodes have been demonstrated to provide substantially greater signal stability and consistency, even across limb positions [36]. However, micro movement of electrodes and variation in tissue impedance on stimulation artifacts due to limb position changes remains unknown and lies beyond the scope of this work [37]. The participant's neuromusculoskeletal interface has been in continuous use for over four years, and implanted electrodes are known to provide substantially greater stability than surface EMG. Long-term investigations of comparable systems have demonstrated stable electrode impedance over 123 weeks [11]. Although short-term baseline drift is therefore unlikely, periodic recalibration may further enhance robustness for slow, long-term changes in electrode impedance that may develop over several months [38]. The consistency of implanted electrodes may extend to stimulation artifacts, although it is possible that inter-electrode distances may shift during certain limb movements; if so, incorporating limb position as an additional parametric input to our proposed SAR method may address this issue, similar to work incorporating limb position into hand posture prediction [39]. The two electrode types used by our study participant (epimysial and intramuscular) may also deserve further consideration. Although both electrode types yield a similar signal-to-noise ratio and thus are expected to provide equal performance when controlling a prosthesis, greater cross-channel impedance ratios may indicate intramuscular electrodes as less susceptible to stimulation artifacts compared to epimysial electrodes [40]. Nonetheless, the impacts of limb position and electrode configuration on stimulation artifacts lies beyond the scope of this work. Evaluating multi-day stability and the feasibility of online adaptation under embedded resource constraints represents an important next step toward clinical translation. Incorporating additional physiological regressors, such as limb position, contraction intensity, or impedance fluctuations, may further enhance robustness. Importantly, such modest model extensions would require only a few additional regression parameters and are unlikely to impose substantial memory or computational demands on the embedded system [41].

Future work should evaluate the stability of the regression model over extended timescales and under more variable limb positions and contraction intensities. Incorporating additional physiological regressors, such as limb position or impedance fluctuations, could further enhance robustness in naturalistic scenarios. Lightweight online recalibration strategies or adaptive filtering approaches may provide efficient compensation for slow baseline drift while remaining compatible with the constraints of embedded systems. Collecting data across multiple participants, electrode types, and stimulation conditions will be important to confirm generalizability and guide optimization for clinical deployments.

V. Conclusion

This study introduced and validated a real-time filtering algorithm designed to mitigate stimulation artifacts during amplitude-modulated nerve stimulation in EMG signals from implanted electrodes. Unlike existing methods, the proposed solution dynamically models artifacts as a function of stimulation amplitude, enabling artifact removal even under conditions of continuous modulation—an essential requirement for simultaneous control and sensory feedback in closed-loop prosthetic systems.

The algorithm was implemented on an embedded prosthesis controller and evaluated both offline and in real-time motion classification tests. Results demonstrated that the filter successfully restored key EMG signal features and significantly improved classification performance, with completion rates tripling under fixed stimulation and increasing by 12% under modulated conditions. While residual artifacts persisted, particularly in rest periods and during modulation, the approach outperformed unfiltered control and preserved critical signal characteristics necessary for reliable prosthetic use.

These findings provide evidence that real-time, regression-based artifact modeling is a potential viable strategy for managing dynamic neurostimulation in neuroprostheses. Future work should focus on increasing filter adaptability to physiological variability and extending the model to handle multi-parametric stimulation. This approach lays the groundwork for more robust, high-performance bidirectional prostheses integrating stable control and sensory feedback.

Acknowledgment

The authors would like to thank Jan Zbinden for his support during the patient visits. They also would like to thank Mirka Buist for help with graphical design in Figure 1. Max Ortiz-Catalan consulted for Integrum AB. All participants provided written informed consent prior to participation in the study.

References

[1] A. Marinelli et al., "Active upper limb prostheses: A review on current state and upcoming breakthroughs," *Prog. Biomed. Eng.*, vol. 5, no. 1, Jan. 2023, Art. no. 012001, doi: 10.1088/2516-1091/acac57.

[2] D. Farina et al., "Toward higher-performance bionic limbs for wider clinical use," *Nature Biomed. Eng.*, vol. 7, no. 4, pp. 473–485, May 2021, doi: 10.1038/s41551-021-00732-x.

[3] L. E. Osborn, M. M. Iskarous, and N. V. Thakor, "Sensing and control for prosthetic hands in clinical and research applications," in *Wearable Robotics*. Amsterdam, The Netherlands: Elsevier, 2020, pp. 445–468, doi: 10.1016/B978-0-12-814659-0.00022-9.

[4] A. D. Roche et al., "Upper limb prostheses: Bridging the sensory gap," *J. Hand Surg. Eur.*, vol. 48, no. 3, pp. 182–190, Mar. 2023, doi: 10.1177/17531934221131756.

[5] Y. Jiang, M. Togane, B. Lu, and H. Yokoi, "SEMG sensor using polypyrrole-coated nonwoven fabric sheet for practical control of prosthetic hand," *Front Neurosci.*, vol. 11, p. 33, Aug. 2017, doi: 10.3389/fnins.2017.00033.

[6] W. Daly, L. Voo, T. Rosenbaum-Chou, A. Arabian, and D. Boone, "Socket pressure and discomfort in upper-limb prostheses: A preliminary study," *JPO, J. Prosthetics Orthotics*, vol. 26, no. 2, pp. 99–106, 2014.

[7] S. Salminger et al., "Current rates of prosthetic usage in upper-limb amputees—Have innovations had an impact on device acceptance?," *Disability Rehabil.*, vol. 44, no. 14, pp. 3708–3713, Jul. 2022, doi: 10.1080/09638288.2020.1866684.

[8] M. Ortiz-Catalan, B. Håkansson, and R. Brånemark, "An osseointegrated human-machine gateway for long-term sensory feedback and motor control of artificial limbs," *Sci. Translational Med.*, vol. 6, no. 257, p. 257, Oct. 2014, doi: 10.1126/scitranslmed.3008933.

[9] M. Ortiz-Catalan, E. Mastinu, P. Sassu, O. Aszmann, and R. Brånemark, "Self-contained neuromusculoskeletal arm prostheses," *New England J. Med.*, vol. 382, no. 18, pp. 1732–1738, Apr. 2020, doi: 10.1056/nejmoa1917537.

[10] E. Mastinu, R. Brånemark, O. Aszmann, and M. Ortiz-Catalan, "Myoelectric signals and pattern recognition from implanted electrodes in two TMR subjects with an osseointegrated communication interface," in *Proc. 40th Annu. Int. Conf. IEEE Eng. Med. Biol. Soc. (EMBC)*, Jul. 2018, pp. 5174–5177, doi: 10.1109/EMBC.2018.8513466.

[11] M. Ortiz-Catalan et al., "A highly integrated bionic hand with neural control and feedback for use in daily life," *Sci. Robot.*, vol. 8, no. 83, p. 7360, Oct. 2023, doi: 10.1126/scirobotics.adf7360.

[12] J. Zbinden et al., "Improved control of a prosthetic limb by surgically creating electro-neuromuscular constructs with implanted electrodes," *Sci. Transl. Med.*, vol. 15, no. 704, Jul. 2023, Art. no. eabq3665, doi: 10.1126/scitranslmed.abq3665.

[13] J. Cheesborough, L. Smith, T. Kuiken, and G. Dumanian, "Targeted muscle reinnervation and advanced prosthetic arms," *Seminars Plastic Surg.*, vol. 29, no. 1, pp. 62–72, Feb. 2015, doi: 10.1055/s-0035-1544166.

[14] E. N. Morgan, B. K. Potter, J. M. Souza, S. M. Tintle, and G. P. Nanos, "Targeted muscle reinnervation for transradial amputation: Description of operative technique," *Techn. Hand Upper Extremity Surg.*, vol. 20, no. 4, pp. 166–171, Dec. 2016, doi: 10.1097/bth.0000000000000141.

[15] A. R. Walsh, J. Lu, E. Rodriguez, S. Diamond, and S. M. Sultan, "The current state of targeted muscle reinnervation: A systematic review," *J. Reconstructive Microsurgery*, vol. 39, no. 3, pp. 238–244, Mar. 2023, doi: 10.1055/s-0042-1755262.

[16] M. Ortiz-Catalan, R. Brånemark, B. Håkansson, and J. Delbeke, "On the viability of implantable electrodes for the natural control of artificial limbs: Review and discussion," *Biomed. Eng. OnLine*, vol. 11, no. 1, p. 33, Jun. 2012, doi: 10.1186/1475-925x-11-33.

[17] E. J. Earley and M. Ortiz-Catalan, "Neurostimulation perception obeys strength-duration curves and is primarily driven by pulse amplitude," in *Proc. 11th Int. IEEE/EMBS Conf. Neural Eng. (NER)*, Apr. 2023, pp. 1–5, doi: 10.1109/NER52421.2023.10123893.

[18] C. Hartmann, S. Dosen, S. Amsuess, and D. Farina, "Closed-loop control of myoelectric prostheses with electrotactile feedback: Influence of stimulation artifact and blanking," *IEEE Trans. Neural Syst. Rehabil. Eng.*, vol. 23, no. 5, pp. 807–816, Sep. 2015, doi: 10.1109/TNSRE.2014.2357175.

[19] E. J. Earley, A. Berneving, J. Zbinden, and M. Ortiz-Catalan, "Neurostimulation artifact removal for implantable sensors improves signal clarity and decoding of motor volition," *Frontiers Hum. Neurosci.*, vol. 16, Oct. 2022, Art. no. 1030207, doi: 10.3389/fnhum.2022.1030207.

[20] S. Kanoga, Y. Mitsukura, S. Kanoga, and Y. Mitsukura, "Review of artifact rejection methods for electroencephalographic systems," in *Electroencephalography*. Rijeka, Croatia: IntechOpen, 2017, pp. 69–89, doi: 10.5772/68023.

[21] Y. Chen, B. Ma, H. Hao, and L. Li, "Removal of electrocardiogram artifacts from local field potentials recorded by sensing-enabled neurostimulator," *Front Neurosci.*, vol. 15, Apr. 2021, Art. no. 637274, doi: 10.3389/fnins.2021.637274.

[22] J. M. Weiss, S. N. Flesher, R. Franklin, J. L. Collinger, and R. A. Gaunt, "Artifact-free recordings in human bidirectional brain–computer interfaces," *J. Neural Eng.*, vol. 16, no. 1, Nov. 2018, Art. no. 016002, doi: 10.1088/1741-2552/aae748.

[23] A. Zhou, B. C. Johnson, and R. Müller, "Toward true closed-loop neuromodulation: Artifact-free recording during stimulation," *Current Opinion Neurobiol.*, vol. 50, pp. 119–127, Jun. 2018, doi: 10.1016/j.conb.2018.01.012.

[24] S. Abbaspour and A. Fallah, "Removing ECG artifact from the surface EMG signal using adaptive subtraction technique," *J. Biomed. Phys. Eng.*, vol. 4, no. 1, pp. 33–38, Mar. 2014.

[25] K. Gunasekaran, V. D. A. Kumar, and A. M. Judith, "Artifact removal from ECG signals using online recursive independent component analysis," *J. Comput. Math. Data Sci.*, vol. 13, Dec. 2024, Art. no. 100102, doi: 10.1016/j.jcmds.2024.100102.

[26] D. T. O'Keeffe, G. M. Lyons, A. E. Donnelly, and C. A. Byrne, "Stimulus artifact removal using a software-based two-stage peak detection algorithm," *J. Neurosci. Methods*, vol. 109, no. 2, pp. 137–145, Aug. 2001, doi: 10.1016/s0165-0270(01)00407-1.

[27] F. Clemente, M. D'Alonzo, M. Controzzi, B. B. Edin, and C. Cipriani, "Non-invasive, temporally discrete feedback of object contact and release improves grasp control of closed-loop myoelectric transradial prostheses," *IEEE Trans. Neural Syst. Rehabil. Eng.*, vol. 24, no. 12, pp. 1314–1322, Dec. 2016, doi: 10.1109/TNSRE.2015.2500586.

[28] F. Mandrile, D. Farina, M. Pozzo, and R. Merletti, "Stimulation artifact in surface EMG signal: Effect of the stimulation waveform, detection system, and current amplitude using hybrid stimulation technique," *IEEE Trans. Neural Syst. Rehabil. Eng.*, vol. 11, no. 4, pp. 407–415, Dec. 2003, doi: 10.1109/TNSRE.2003.819791.

[29] B. Hudgins, P. Parker, and R. N. Scott, "A new strategy for multifunction myoelectric control," *IEEE Trans. Biomed. Eng.*, vol. 40, no. 1, pp. 82–94, Jan. 1993, doi: 10.1109/10.204774.

[30] E. Scheme and K. Englehart, "Training strategies for mitigating the effect of proportional control on classification in pattern recognition–based myoelectric control," *JPO J. Prosthetics Orthotics*, vol. 25, no. 2, pp. 76–83, Apr. 2013, doi: 10.1097/jpo.0b013e318289950b.

[31] T. A. Kuiken, "Targeted muscle reinnervation for real-time myoelectric control of multifunction artificial arms," *JAMA*, vol. 301, no. 6, p. 619, Feb. 2009, doi: 10.1001/jama.2009.116.

[32] M. Ortiz-Catalan, R. Brånemark, and B. Håkansson, "BioPatRec: A modular research platform for the control of artificial limbs based on pattern recognition algorithms," *Source Code Biol. Med.*, vol. 8, pp. 1–18, Aug. 2013, doi: 10.1186/1751-0473-8-11.

[33] J. Chen, M. Jiang, X. Zhang, D. S. da Silva, V. H. C. de Albuquerque, and W. Wu, "Implementing ultra-lightweight co-inference model in ubiquitous edge device for atrial fibrillation detection," *Expert Syst. Appl.*, vol. 216, Apr. 2023, Art. no. 119407, doi: 10.1016/j.eswa.2022.119407.

[34] E. Park, J. Ahn, and S. Yoo, "Weighted-entropy-based quantization for deep neural networks," in *Proc. IEEE Conf. Comput. Vis. Pattern Recognit. (CVPR)*, Jul. 2017, pp. 7197–7205, doi: 10.1109/CVPR.2017.761.

[35] E. Campbell, A. Phinyomark, and E. Scheme, "Current trends and confounding factors in myoelectric control: Limb position and contraction intensity," *Sensors*, vol. 20, no. 6, p. 1613, Mar. 2020, doi: 10.3390/s20061613.

[36] E. Mastinu et al., "Grip control and motor coordination with implanted and surface electrodes while grasping with an osseointegrated prosthetic hand," *J. NeuroEng. Rehabil.*, vol. 16, no. 1, p. 49, Dec. 2019, doi: 10.1186/s12984-019-0511-2.

[37] D. W. Tan, M. A. Schiefer, M. W. Keith, J. R. Anderson, J. Tyler, and D. J. Tyler, "A neural interface provides long-term stable natural touch perception," *Sci. Transl. Med.*, vol. 6, no. 257, Oct. 2014, Art. no. 257ra138, doi: 10.1126/scitranslmed.3008669.

[38] P. P. Vu et al., "Long-term upper-extremity prosthetic control using regenerative peripheral nerve interfaces and implanted EMG electrodes," *J. Neural Eng.*, vol. 20, no. 2, Apr. 2023, Art. no. 026039, doi: 10.1088/1741-2552/accb0c.

[39] A. A. Adewuyi, L. J. Hargrove, and T. A. Kuiken, "Resolving the effect of wrist position on myoelectric pattern recognition control," *J. NeuroEngineering Rehabil.*, vol. 14, no. 1, p. 39, May 2017, doi: 10.1186/s12984-017-0246-x.

[40] E. J. Earley, M. B. Kristoffersen, and M. Ortiz-Catalan, "Comparing implantable epimysial and intramuscular electrodes for prosthetic control," *Frontiers Neurosci.*, vol. 19, Jun. 2025, Art. no. 1568212, doi: 10.3389/fnins.2025.1568212.

[41] F. Just, C. Ghinami, J. Zbinden, and M. Ortiz-Catalan, "Deployment of machine learning algorithms on resource-constrained hardware platforms for prosthetics," *IEEE Access*, vol. 12, pp. 40439–40449, 2024, doi: 10.1109/ACCESS.2024.3371251.